

Magnesiostauroilite and zincostauroilite: mineral description with a petrogenetic and crystal-chemical update*

CHRISTIAN CHOPIN¹⁺, BRUNO GOFFE¹, LUCIANO UNGARETTI^{2,3} and ROBERTA OBERTI²

¹ Laboratoire de Géologie, UMR 8538 du CNRS, Ecole normale supérieure, 24 rue Lhomond, F-75005 Paris, France
+ corresponding author, e-mail: chopin@geologie.ens.fr

² CNR Istituto di Geoscienze e Georisorse (IGG), via Ferrata 1, I-27100 Pavia, Italy

³ Dipartimento di Scienze della Terra, Università di Pavia, via Ferrata 1, I-27100 Pavia, Italy

Abstract: Magnesiostauroilite, ideally ${}^A\Box_4 {}^B\text{Mg}_4 {}^C\text{Al}_{16} {}^D(\text{Al}_2\Box_2) {}^T\text{Si}_8 \text{O}_{40} {}^X[(\text{OH})_2\text{O}_6]$, occurs together with talc, clinocllore and kyanite (or alone, armouring corundum) as inclusions in pyrope megablasts from the ultra-high-pressure metamorphic terrane of the Dora-Maira massif, Italian Western Alps. It is transparent colourless in thin section; non pleochroic, biaxial with a $2V$ angle close to 90° ; the birefringence is low (< 0.010) with a mean value of $n = 1.709(2)$ at 592 nm. A few crystals show a 'tweed' texture under crossed nicols. The calculated density is 3.54 g/cm^3 . Zincostauroilite, ideally ${}^A\Box_4 {}^B\text{Zn}_4 {}^C\text{Al}_{16} {}^D(\text{Al}_2\Box_2) {}^T\text{Si}_8 \text{O}_{40} {}^X[(\text{OH})_2\text{O}_6]$, occurs with kyanite, muscovite, margarite, \pm chloritoid, gahnite and either quartz or diaspore in a karst-filling meta-argillite of the Mesozoic Barrhorn series, Zermatt valley, Swiss Western Alps; it may have formed concurrently with kyanite from the breakdown of gahnite + pyrophyllite + diaspore, *i.e.* near 400°C . Zincostauroilite is non pleochroic and biaxial positive, with positive elongation ($\gamma = c$); $\alpha = 1.722(2)$ and $\gamma = 1.734(2)$ at 592 nm. The calculated density is 3.78 g/cm^3 . Both magnesiostauroilite and zincostauroilite samples are monoclinic, $C2/m$, with the β angle equal or very close to 90° , which implies a very low degree of cation order; this feature is confirmed by the nearly equal site-scattering values and the similar mean bond lengths refined at the relevant pairs of sites; it is unrelated to metamorphic grade. Electron and ion microprobe analyses were combined to new single-crystal structure refinements to give the following crystal-chemical formulae: magnesiostauroilite, ${}^A(\text{Fe}^{2+}_{0.16}\text{Mg}_{0.72}\Box_{3.12}) {}^B(\text{Mg}_{1.86}\text{Li}_{0.94}\text{Zn}_{0.02}\Box_{1.18}) {}^C(\text{Al}_{15.96}\text{Ti}_{0.04}) {}^D(\text{Al}_{1.58}\text{Mg}_{0.45}\Box_{1.97}) {}^T(\text{Si}_{7.96}\text{Al}_{0.04}) \text{O}_{40} {}^X[(\text{OH})_{3.98}\text{O}_{4.02}]$; zincostauroilite, ${}^A(\text{Fe}^{2+}_{0.13}\text{Mg}_{0.10}\Box_{3.77}) {}^B(\text{Zn}_{2.45}\text{Li}_{0.51}\text{Fe}^{2+}_{0.20}\Box_{0.84}) {}^C(\text{Al}_{15.98}\text{Ti}_{0.02}) {}^D(\text{Al}_{1.95}\text{Mg}_{0.09}\Box_{1.96}) {}^T\text{Si}_8 \text{O}_{40} {}^X[(\text{OH})_{3.67}\text{O}_{4.33}]$. The magnesiostauroilite crystal, with several hundreds ppm BeO, probably shows the highest Li and Be contents ever measured in staurolite. The increased occupancy of the M4 octahedron at the expense of the T2 tetrahedron from Fe- or Zn-rich to Mg-rich staurolite may be the key to the Mg-staurolite paradox (a high-pressure phase with expectedly four-fold coordinated Mg) and to the complex thermodynamic behaviour of the staurolite series (*e.g.* reversal in Fe-Mg partitioning with garnet).

Key-words: magnesiostauroilite, zincostauroilite, staurolite group, new mineral, high-pressure phase, order-disorder, lithium, beryllium.

Introduction

The iron-aluminium silicate staurolite is a long-known and common mineral in intermediate-grade metamorphic rocks; its crystal chemistry has yet been a persisting source of perplexity until the formidable study of Hawthorne *et al.* (1993a, b and c), after Lonker (1983) had demonstrated the variability of the number of protons and Dutrow *et al.* (1986) had shown that lithium may be a major though not essential constituent of it. An uncommon feature of this silicate is the presence of a tetrahedral site (T2) occupied by divalent cations (essentially Fe^{2+}). For crystal-field stabilization reasons such a site is favoured by the Zn^{2+} ions and makes staurolite (and spinel at lower and higher grade) a sink for all the zinc contained in the rock. Indeed, ZnO contents of several weight percents are commonly recorded in staurolite, in a few instances up to values making Zn^{2+} al-

most (Soto & Azañon, 1994) or actually [Leupolt & Franz, 1986; in Sartori, 1988; Soto & Azañon, 1993 (up to 13.1 wt%); Oberti *et al.*, 1996 (11.1 wt%); Feenstra *et al.*, 2002 (12.9 wt%)] the dominant divalent cation. Other divalent cations known are cobalt, dominant in lusakite (Skerl & Bannister, 1934; *cf.* Čech *et al.*, 1981), and magnesium, the latter in relatively high-pressure rocks (Grew & Sandiford, 1984; Schreyer *et al.*, 1984; Ward, 1984; Smith, 1988) in which it may become dominant (Nicollet, 1986; Enami & Zang, 1988; Gil Ibarguchi *et al.*, 1991; Chopin *et al.*, 1993; Peacock & Goodge, 1995). An interesting paradox is that the formation of magnesian staurolite from low-pressure precursors like chlorite implies a *decreasing* coordination of Mg with increasing pressure, should this element occupy the same site as Fe and Zn. A detailed investigation of the site preference of Fe, Co, Zn and Mg in staurolite by means of EXAFS analysis has been reported by Henderson *et al.* (1997).

* We dedicate this paper to the memory of our co-author Luciano Ungaretti, a good friend and outstanding mineralogist.

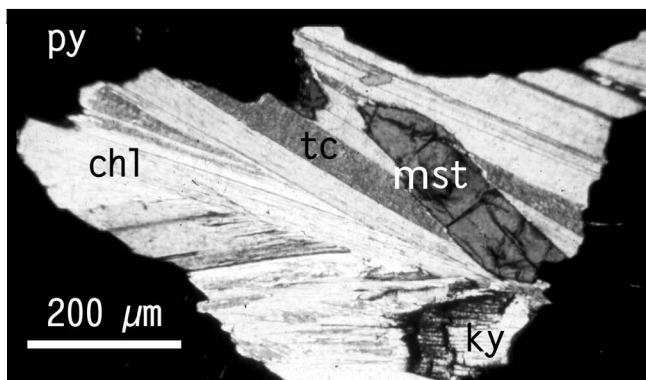


Fig. 1. Polyminerally inclusion of magnesio-stauriolite (mst), inter-leaved clinocllore (chl) and talc (tc), and kyanite (ky, partly pulled out) within a megacryst of pyrope garnet (py). Photomicrograph, crossed nicols; sample 85DM66b, Val Gilba, Dora-Maira massif. The relevant assemblage in the MASH system is invariant.

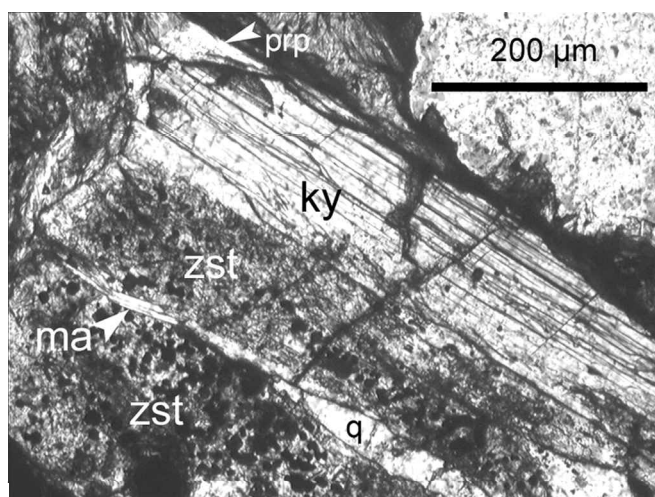


Fig. 2. Photomicrograph of the Barrhorn meta-argillite, showing zincostauriolite (zst, in parallel growth with kyanite, ky) crowded with inclusions of pyrite except for a clear rim, quartz (q) and margarite (ma), in a dark groundmass of muscovite. Note the late growth of pyrophyllite (prp) on kyanite. The light area in the upper right corner is a hole. Sample Barr888, plane polarized light.

We report in this paper the complete description of the two stauriolite samples that provoked approval of the two end-member names by the IMA-CNMMN (votes 92-035/036) and the structure of which was refined by Hawthorne *et al.* [1993a, samples S(41) and S(42)]. The ideal compositions of these end-members are: $A\text{Al}_4\text{B}^{\text{Mg}}\text{CAl}_{16}\text{D}(\text{Al}_2\text{Si}_2)\text{Si}_8\text{O}_{40}\text{X}[(\text{OH})_2\text{O}_6]$ for magnesio-stauriolite and $A\text{Al}_4\text{B}^{\text{Zn}}\text{CAl}_{16}\text{D}(\text{Al}_2\text{Si}_2)\text{Si}_8\text{O}_{40}\text{X}[(\text{OH})_2\text{O}_6]$ for zincostauriolite, referring to Hawthorne *et al.* (1993a) for the site nomenclature. Type material for both species has been deposited at the Ecole des Mines de Paris under sample numbers 56244 and 56245, respectively.

Crystal-chemical formulae were revisited on the basis of new structure refinements, and the problem of order-disorder in stauriolite is addressed in the light of new findings and of recent literature.

Occurrence and paragenesis

Magnesio-stauriolite. The mineral occurs exclusively as inclusions in pyrope megacrysts from the coesite-bearing metamorphic terrane in the Dora-Maira massif, Italian Western Alps, especially in the Vallone di Gilba, Val Varaita. Details on the geology and petrology of the area can be found in Chopin *et al.* (1991), Compagnoni *et al.* (1995) and Chopin & Schertl (1999). The mineral formed more or less coevally with the pyrope megacrysts at conditions between 25–32 kbar and 700–750°C, during Alpine regional very-high-pressure metamorphism. Closer petrographic inspection reveals three types of occurrence (Simon *et al.*, 1997; Simon & Chopin, 2001). i) In homogeneous near-end-member pyrope megacrysts, magnesio-stauriolite is typically associated with talc, clinocllore, kyanite and rutile in polyminerally inclusions (Fig. 1), as in the holotype sample (85DM66b, in which magnesiodumortierite also occurs, Chopin *et al.*, 1995). ii) In a few other homogeneous near-end-member pyrope megacrysts, magnesio-stauriolite occurs as single-crystal inclusions that contain armoured relics of corundum; magnesiochloritoid also occurs in these garnet megacrysts. iii) In colour- and Fe-Mg zoned, ellenbergerite-bearing pyrope megacrysts, magnesio-stauriolite occurs both as a primary phase along with magnesiochloritoid, kyanite and talc, and as a later breakdown product associated with chlorite (\pm corundum) in symplectites replacing magnesiochloritoid (Fig. 4c–d in Simon *et al.*, 1997).

Zincostauriolite. The mineral occurs in a metabasite pocket of the Mesozoic Barrhorn series, Zermatt valley, Swiss Western Alps (Sartori, 1988). The dense, hard, finely equigranular rock with rusty patina and dark blue-green fracture forms a layer of about 50 m extension and up to 2 m thickness on the eastern side of the Turtmannletscher (3270 m), where it pinches out toward the Bruneggjoch (Swiss map coordinates 622.925/109.175). It represents a former karst-filling argillite (grading into bauxite) within the calcite and dolomite marbles of the Middle Triassic, and is discordantly overlain by the Malm marbles (Sartori, 1988). [It is therefore in the same position as the Mn-rich pocket in which turtmannite was discovered (Brugger *et al.*, 2001)]. The rock-forming minerals are abundant muscovite, stauriolite *s.l.*, kyanite and margarite, with or without the lithian chlorite cookeite, chloritoid, diaspore (sometimes only as armoured relics in stauriolite), paragonite, the near-end-member zinc spinel gahnite (2 wt% FeO), accessory rutile, apatite, pyrite and zircon, in a few instances allanite, a REE-Al-phosphate (florencite?), ankerite or tourmaline. Pyrophyllite and kaolinite (probably also sudoite) are late products in the matrix; cookeite also occurs as thin cross-cutting veinlets. The holotype sample Barr888 is the only one containing minor quartz, beside muscovite, margarite, stauriolite *s.l.*, kyanite, pyrite, rutile, tourmaline, zircon and late pyrophyllite (Fig. 2). Petrological investigation indicates that zincostauriolite formed during regional Alpine metamorphism at about 400–450°C and 3–8 kbar, as implied by the coexistence of kyanite, diaspore and cookeite (*cf.* Vidal & Goffé, 1991) in some samples and of margarite and quartz in the holotype. Lower-grade, high-pressure stratigraphic equivalents of this karstic filling in Vanoise and Liguria,

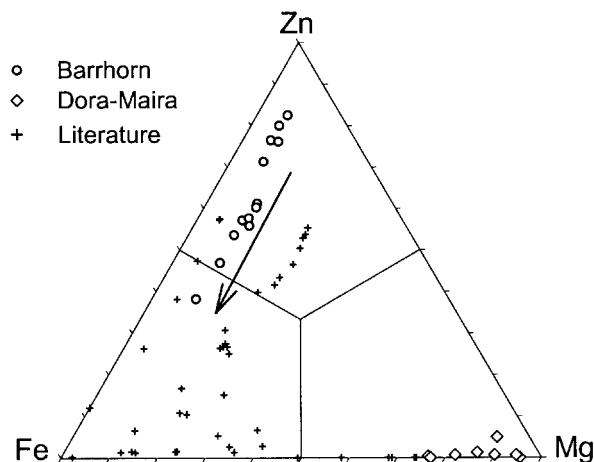


Fig. 3. Compositional variations in the staurolite group in terms of relative proportions of the main divalent cations. Data sources in the text, and unpublished data of the authors for the Barrhorn and Dora-Maira samples. The arrow indicates core to rim zonation in zincostauroilite crystals from Barrhorn. The subdivisions drawn are a practical distinction (as long as Li is not dominant) between staurolite proper, zincostauroilite and magnesiostauroilite on the basis of the dominant divalent cations — considered as essentially occupying the T2 site, regardless of their minor occupancies and partitioning between octahedral sites.

French and Italian Western Alps, respectively, contain pyrophyllite, diaspore, chloritoid, Fe-Mg-carpholite, cookeite, lawsonite and gahnite, but neither staurolite nor kyanite nor margarite (Goffé & Saliot, 1977; Goffé, 1980, 1984; Goffé & Velde, 1984; Poinssot *et al.*, 1997).

Physical and optical properties

In the holotype sample, *magnesiostauroilite* is found as rare anhedral isolated grains with size ranging from a few tens to 250 μm . It was only detected in thin section, where it appears colourless, transparent and non fluorescent. The largest crystal (Fig. 1) was drilled out after electron- and ion-microprobe work, broken into two pieces, one of which served for optical measurements, the other for X-ray diffraction work. Because of the small grain size, several properties could not be determined; however, based on its chemistry, magnesiostauroilite should have a white streak, a vitreous to resinous lustre and H values around 7–7.5. The calculated density is 3.54 g/cm^3 . Magnesiostauroilite is non pleochroic, biaxial with a $2V$ angle close to 90° . Because of the low birefringence and the poor optical quality, only a mean value of n , 1.709(2) at 592 nm, could be obtained with a spindle stage equipped with a refractometer. Crystals are untwinned but in a few samples a ‘tweed’ texture was observed under crossed nicols (Simon *et al.*, 1998, and in prep.).

Zincostauroilite occurs as prismatic crystals up to 3 mm long, mostly untwinned. They contain minute inclusions of pyrite and rutile, and are commonly sandwiched between kyanite crystals in parallel growth (Fig. 2), with (010) of zincostauroilite parallel to (100) of kyanite. Zinco-

stauroilite is colourless in thin section. Its streak, lustre and hardness should be similar to those proposed for magnesiostauroilite. Reliable measurements of the density could not be obtained due to impressive chemical zoning and abundant inclusions; the calculated density is 3.78 g/cm^3 . After electron-microprobe reconnaissance work on a dozen samples had shown a broad range of Fe- to Zn-rich staurolite compositions (typically $X_{\text{Zn}} = \text{Zn}/(\text{Zn} + \text{Fe} + \text{Mg})$ between 0.8 and 0.45 within crystal, from core to rim; Fig. 3), a large crystal free of kyanite intergrowths was selected in sample Barr888 (holotype) for the high Zn contents in its core. This core was drilled out of the thin section for optical and X-ray work. Zincostauroilite is non pleochroic and biaxial positive, with positive elongation ($\gamma = c$). Due to the poor optical quality of the crystal extracted, no extinction curve could be obtained with the spindle stage; the extreme indices measured are $\alpha = 1.722(2)$ and $\gamma = 1.734(2)$ at 592 nm.

Mineral chemistry

Analytical techniques: Electron microprobe analyses of these two crystals were obtained with a Camebax Microbeam apparatus, Paris 6 University (15 kV, 15 nA, 10 to 20 s counting time on peak and on background, PAP data reduction program). The standards used were forsterite (Mg, Si), anorthite (Al, Ca), Fe_2O_3 (Fe), MnTiO_3 (Mn, Ti) and ZnS (Zn) for magnesiostauroilite, and almandine (Al, Si, Fe), forsterite (Mg), ZnS (Zn) and MnTiO_3 (Mn, Ti) for zincostauroilite. Fluorine was close to the detection limit (~ 0.1 wt%) and no other element was detected. The average of three analyses in clear areas of each crystal is reported in Table 1.

The magnesiostauroilite crystal and an other zincostauroilite crystal from the same, holotype sample were subsequently analysed by ion microprobe using the Cameca IMS3f instrument then (in 1987–88) at Institut für Petrographie und Geochemie, Karlsruhe University. The ^7Li , ^9Be and ^{28}Si counts were collected 60 or 100 times for one second on each point using a primary mass-separated beam of $^{16}\text{O}^-$ ions of 10 keV, a 2 nA (magnesiostauroilite) or 5 nA (zincostauroilite) beam current and measuring energy-filtered positive ions. A calibration curve for Li was obtained by concurrent measurements of the $^7\text{Li}/^{28}\text{Si}$ count ratio on the 77–55c iron-rich staurolite standard (0.56 wt% Li_2O by ion microprobe, Holdaway *et al.*, 1986; cf. the 0.62 wt% atomic-absorption value reported by Dutrow *et al.*, 1986), on cookeite, spodumene and petalite (nominal Li contents), and normalization to the silica weight percents as determined by electron microprobe. The regression curve forced through the origin has an R^2 value of 0.985 (0.999 if the H_2O -rich phase cookeite is ignored), a gratifying result if one considers the unknown matrix effects in the variety of standards used. It is yet unlikely (or fortuitous) that the accuracy of the ion-microprobe results was better than 10 percent for Li (and, conservatively, 20 percent for Be for which only one standard, beryl, was available).

Two traverses were made across the magnesiostauroilite crystal and revealed a distinct zonation of the Li contents, with a central plateau bounded by maxima in the inner rim and minima in the outer rim. Three point analyses were

Table 1. Electron and ion microprobe analyses (averaged over 3 points) and unit formulae recalculated on the basis of 48 oxygen atoms, with H calculated to obtain Si contents consistent with the observed <T1-O> distances.

Magnesiostauroilite				Zincostauroilite		
cation	oxide wt%	range	apfu	oxide wt%	range	apfu
Si ⁴⁺	30.66	30.6–30.7	7.959	28.47	28.1–28.8	8.000
Al ³⁺	57.45	57.3–57.8	17.578	54.12	54.0–54.9	17.926
Ti ⁴⁺	0.18	0.16–0.23	0.035	0.11	0.05–0.22	0.023
Fe ²⁺	0.72	0.66–0.76	0.156	1.40	1.33–1.92	0.329
Mg ²⁺	7.77	7.70–7.84	3.007	0.45	0.44–0.49	0.189
Mn ²⁺	–	–	–	0.01	0.00–0.02	0.002
Zn ²⁺	0.10	0.05–0.12	0.019	11.82	11.6–12.1	2.453
Li ⁺	0.90	0.6–1.2	0.940	0.45		0.509
H ⁺	(2.30)		3.983	(1.96)		3.674
wt%	100.08			98.79		
sum			29.694			29.449
catsum *						

* catsum is the sum of non-H cations, a parameter used by Hawthorne *et al.* (1993c) to empirically evaluate the H content in staurolite

made, one in the core [0.57(3) wt% Li₂O], two in the inner rims [1.64(8) and 0.71(3) wt% Li₂O]. No variation in the major elements was observed that could be correlated with this zonation. The Li₂O value reported in Table 1 is the average along the traverse, thought to be representative of the bulk crystal. It is among the highest values known in staurolite (*cf.* Hawthorne *et al.*, 1993a). The zincostauroilite analysed contains 0.45 wt% Li₂O, and the coexisting tourmaline 0.30 wt%, showing once more that staurolite is a major Li carrier in metasediments. Even more surprising are, in view of the reported absence or low contents of beryllium in the surveys of Dutrow *et al.* (1986), Holdaway *et al.* (1986) and Grew (2002), the several hundreds ppm BeO found in the magnesiostauroilite crystal and in the Fe-Li-rich standard 77-55c. The ⁹Be⁺ measurements being complicated by possible interference with ²⁷Al³⁺ (Grew *et al.*, 1986), we conservatively accounted for the latter assuming that the very low counts obtained on mass 9 for zincostauroilite, kyanite and chloritoid are entirely due to the Al contribution, leading to a ²⁷Al³⁺ / ²⁷Al⁺ ratio of 3.6 · 10⁻⁵ (*cf.* 5 · 10⁻⁵ for Grew *et al.*, 1986). This ratio was then used to correct for interference on mass 9, leading to BeO contents of 200 to 380 ppm on the three grains of staurolite standard 77-55c. For magnesiostauroilite, beryllium was not directly measured but a scan of the low mass numbers made on a point in the inner rim of the crystal showed strong signals for masses 7, 8 and 9, the latter converting into 110 to 600 ppm BeO after correction for Al contribution (and reference to ²⁸Si counts through the ⁹Be/^{Li} ratio of the scan and the ⁷Li/²⁸Si ratios of the point analyses).

The H₂O wt% values reported in Table 1 have been calculated to obtain a reasonable consistency between the Si content and the measured <T1-O> distances, as well as between the CATSUM index and the H content (Hawthorne *et al.*, 1993a and c, respectively). For magnesiostauroilite, 8.0 Si apfu would have been obtained with 3.48 H apfu (2.00 wt%,

Table 2. Selected crystal and refinement data.

	Magnesiostauroilite	Zincostauroilite
<i>a</i> (Å)	7.8706(5)	7.853(6)
<i>b</i> (Å)	16.5411(16)	16.534(9)
<i>c</i> (Å)	5.6323(3)	5.639(5)
β (°)	90.007(4)	90.00(8)
<i>V</i> (Å ³)	733.3	732.2
space group	<i>C2/m</i>	<i>C2/m</i>
θ range (°)	2–35	2–35
<i>hkl</i> range	± <i>h</i> , ± <i>k</i> , <i>l</i>	± <i>h</i> , ± <i>k</i> , <i>l</i>
# all	1113	1665
# obs (<i>I</i> > 3σ _{<i>I</i>})	652	1065
<i>R</i> sym %	5.8	3.3
<i>R</i> all %	8.0	5.7
<i>R</i> obs %	3.5	2.5

yielding an oxide sum of 99.78). Any lower H₂O value would lead to an unrealistic Si content higher than 8 apfu.

In summary, these crystals represent the closest approach to the Mg and Zn end-members of the staurolite group (Fig. 3). Magnesiostauroilite also shows the highest Be and Li contents ever measured in staurolite. Noteworthy are the high hydroxyl and high (maximum) Si contents in both samples; the low Ti contents contrast with those of most staurolite analyses in the literature (typically 0.1 vs. 0.4 wt% TiO₂).

Magnesiostauroilite composition in other samples from the same area shows significant variations according to paragenesis. Primary ones have high Si contents near 8 apfu and X_{Mg} ratios [= Mg/(Mg+Fe+Zn)] in the range 0.70 to 0.96, depending on how pyrope-rich the enclosing garnet is; their X_{Mg} ratio is consistently lower than that of coexisting garnet. Secondary ones associated with clinocllore in symplectites after magnesiochloritoid are distinctly more Al- and Fe-rich (analyses 9 vs. 10–11 in Simon *et al.*, 1997); the most Al-rich of them (with Si as low as 7.0 apfu) may represent metastable products with respect to the less Al-rich crystals that coexist with corundum (Simon *et al.*, 1997, p. 52).

X-ray analysis and structure refinement

The two holotype single crystals that were drilled out from petrographic thin sections are labelled S(41) and S(42) in Hawthorne *et al.* (1993a), to which the reader is referred for the details of data collection and refinement. The two samples were re-refined for this work, and small but significant changes are observed in the results as well as in the final site distribution (*cf.* the following sections for details). Selected crystal data and refinement information are given in Table 2; atom positions, refined site-scattering values (ss, in epfu) and atom displacement parameters are given in Table 3, and selected interatomic distances and angles are given in Table 4¹. Table 5¹ lists the observed and calculated structure factors.

Given the material paucity and the limitations of the Gandolfi technique for a single crystal, the X-ray powder dif-

¹ Tables 4 and 5 can be obtained from the authors or from the EJM data repository, Editorial Office, Paris.

Table 3. Atom coordinates, refined site scattering values (ss, epfu), and equivalent (\AA^2) and anisotropic ($\times 10^4$) displacement factors for the staurolite end-members.

Magnesiostauroilite	site	ss	x/a	y/b	z/c	B_{eq}	β_{11}	β_{22}	β_{33}	β_{12}	β_{13}	β_{23}
	O1A		0.2364(7)	0	0.9658(9)	0.76	34	1	103	0	-5	0
	O1B		0.2346(6)	0	0.5345(9)	0.65	34	2	67	0	-34	0
	O2A		0.2553(4)	0.1617(2)	0.0140(6)	0.30	7	2	38	-2	-4	0
	O2B		0.2543(4)	0.1618(2)	0.4844(6)	0.34	15	3	28	0	-4	1
	O3		0.0027(4)	0.0887(2)	0.2502(6)	0.56	12	2	95	-1	-13	-3
	O4		0.0206(4)	0.2502(2)	0.2508(6)	0.34	18	3	18	0	0	0
	O5		0.5278(4)	0.0979(2)	0.2512(6)	0.37	11	4	31	2	-8	2
	T1	112.0	0.1339(2)	0.1667(1)	0.2494(3)	0.27	4	3	33	1	-4	1
	T2	25.7	0.3917(6)	0	0.2509(12)	1.37	22	4	250	0	-16	0
	M1A	53.6	1/2	0.1734(1)	0	0.43	16	4	33	0	-8	0
	M1B	53.6	1/2	0.1734(1)	1/2	0.43	12	4	42	0	3	0
	M2	105.5	0.2641(2)	0.4099(1)	0.2500(3)	0.44	8	5	48	0	-10	-1
	M3A	13.0	0	0	0	0.49						
	M3B	13.0	0	0	1/2	0.44						
	M4A	6.2	1/2	0	0	0.89						
	M4B	6.4	1/2	0	1/2	1.22						
Zincostauroilite	site	ss	x/a	y/b	z/c	B_{eq}	β_{11}	β_{22}	β_{33}	β_{12}	β_{13}	β_{23}
	O1A		0.2337(3)	0	0.9670(5)	0.71	27	5	75	0	14	0
	O1B		0.2342(3)	0	0.5321(5)	0.68	27	5	68	0	-2	0
	O2A		0.2551(2)	0.1616(1)	0.0153(3)	0.53	18	6	40	0	4	-2
	O2B		0.2552(2)	0.1617(1)	0.4848(3)	0.55	19	6	45	0	3	1
	O3		0.0018(2)	0.0890(1)	0.2493(3)	0.70	14	6	90	-1	4	0
	O4		0.0214(2)	0.2498(1)	0.2500(3)	0.50	18	5	43	2	8	0
	O5		0.5271(2)	0.0988(1)	0.2502(3)	0.52	14	6	45	0	6	0
	T1	112.0	0.1341(1)	0.1665(1)	0.2500(1)	0.43	12	4	41	0	4	0
	T2	80.9	0.3891(1)	0	0.2496(1)	1.04	32	5	137	0	4	0
	M1A	52.5	1/2	0.1736(1)	0	0.51	18	5	41	0	5	0
	M1B	52.8	1/2	0.1736(1)	1/2	0.54	18	6	44	0	5	0
	M2	104.9	0.2633(1)	0.4104(1)	0.2502(1)	0.62	17	6	60	-1	4	0
	M3A	12.3	0	0	0	0.48	11	5	50	0	12	0
	M3B	11.3	0	0	1/2	0.39	12	4	34	0	-1	0
	M4A	2.3	1/2	0	0	0.48						
	M4B	2.4	1/2	0	1/2	0.96						

fraction patterns have been calculated for $\text{MoK}\alpha$ radiation starting from the results of the structure refinement and are reported in Table 6. An experimental $\text{CuK}\alpha$ powder diffraction pattern for synthetic magnesiostauroilite was reported by Koch-Müller *et al.* (1998).

Petrogenesis and mineral stability

Zincostauroilite

Although zincostauroilite can be readily synthesized at high pressure (Griffen, 1981; Koch-Müller *et al.*, 1997), its stability field has not been determined. However, this mineral clearly appears at lower temperatures but also at higher pressures (in the presence of quartz) than do Fe-rich varieties, as shown by its occurrence in terranes in which normal, Zn-poor pelitic compositions are devoid of staurolite ($T \leq 450^\circ\text{C}$: Barrhorn series, Sartori, 1988; Nevado-Filábride Complex of the Betic Cordillera, Soto & Azañon, 1994; — $P \approx 20$ kbar: Eclogite Unit of the Tauern Window, Leupolt & Franz, 1986). The precursor Zn-carrier at lower grade is

most likely gahnite, as shown by its presence as a primary phase in some Barrhorn samples and in lower-temperature (and higher-pressure) equivalents in Vanoise and Liguria (Goffé, 1980). In the latter, gahnite + pyrophyllite + diasporite is a low-temperature assemblage alternative to zincostauroilite + H_2O . The presence of armoured relics of diasporite in zincostauroilite in some Barrhorn samples may be evidence that such a dehydration reaction was operative in staurolite formation; the coeval growth of kyanite with staurolite in these samples (Fig. 2) suggests in addition that zincostauroilite formed at temperatures very close to those of kyanite appearance in these rocks, which is given by the reaction pyrophyllite + diasporite = kyanite + H_2O , *i.e.* near 400°C or less, depending on fluid composition. This stabilizing effect of Zn toward lower T is also well exemplified by the growth zonation of the Barrhorn staurolite, with extremely Zn-rich core compositions (Fig. 3). As to an upper stability limit on the high-temperature side, the stabilizing effect of Zn with respect to Fe has often been proposed for the occurrence of staurolite at anomalously high grade (*e.g.* Stoddard, 1979, with references). Strictly considered, this is disputable inasmuch as Zn preferentially partitions into spi-

Table 6. X-ray (Mo $K\alpha$) powder diffraction patterns calculated from the results of the structure refinements (reflections with $I > 0.05 I_{\max}$).

A – Magnesiostauroelite													B – Zincostauroelite												
2θ	d	I_{tot}	# refl.	h	k	l	I_{cal}	h	k	l	I_{cal}	2θ	d	I_{tot}	# refl.	h	k	l	I_{cal}	h	k	l	I_{cal}		
9.05	4.504	6.4	1	1	3	0	5.7					4.95	8.229	9.1	1	0	2	0	9.1						
9.25	4.407	12.1	2	1	1	1	6.0	-1	1	1	5.8	5.75	7.085	15.3	1	1	1	0	15.3						
9.85	4.139	23.6	1	0	4	0	23.6					9.85	4.139	8.6	1	0	4	0	8.6						
11.50	3.547	14.6	1	2	2	0	9.8					11.50	3.547	9.5	1	2	2	0	9.5						
11.60	3.516	21.6	2	1	3	1	10.1	-1	3	1	9.0	13.40	3.046	11.8	1	1	5	0	8.0						
12.65	3.226	14.6	2	2	0	1	7.8	-2	0	1	6.9	13.60	3.001	60.6	2	2	2	1	30.7	-2	2	1	29.4		
13.60	3.001	20.3	2	2	2	1	10.9	-2	2	1	9.4	14.35	2.845	6.4	1	2	4	0	4.5						
14.30	2.855	4.4	1	2	4	0	4.2					14.50	2.816	15.9	1	0	0	2	14.9						
14.50	2.816	5.0	1	0	0	2	4.5					14.80	2.759	27.1	1	0	6	0	26.9						
14.80	2.759	15.8	1	0	6	0	15.8					15.25	2.678	70.5	2	1	5	1	33.9	-1	5	1	33.6		
15.25	2.678	38.0	2	1	5	1	20.1	-1	5	1	17.9	15.30	2.669	39.8	1	0	2	2	6.0						
15.75	2.594	7.1	1	3	1	0	7.0					16.10	2.538	26.4	2	2	4	1	13.5	-2	4	1	13.0		
16.05	2.545	3.6	1	2	4	1	3.5					17.10	2.390	86.6	2	-1	3	2	42.0	1	3	2	42.0		
17.10	2.390	50.4	2	1	3	2	25.4	-1	3	2	21.6	17.30	2.363	46.2	1	3	3	0	32.2						
17.25	2.370	32.8	1	3	3	0	22.7					17.40	2.349	44.6	2	-3	1	1	18.7	3	1	1	16.6		
17.35	2.356	24.0	2	3	1	1	8.2	-3	1	1	8.2	17.85	2.290	10.9	2	-2	0	2	5.8	2	0	2	5.0		
17.55	2.329	6.8	1	0	4	2	5.3					18.15	2.253	9.6	1	2	6	0	9.4						
17.85	2.290	8.0	2	2	0	2	4.0	-2	0	2	3.6	19.50	2.098	25.4	2	1	7	1	12.9	-1	7	1	12.5		
18.10	2.259	9.5	1	2	6	0	9.3					20.80	1.968	61.4	1	0	6	2	50.0						
19.50	2.098	12.6	2	1	7	1	6.5	-1	7	1	6.1	20.85	1.964	47.8	1	4	0	0	22.8						
20.80	1.968	100.0	2	0	6	2	66.7	4	0	0	33.3	23.10	1.775	4.7	1	4	4	0	4.7						
24.05	1.706	7.6	2	1	9	1	3.9	-1	9	1	3.7	23.55	1.741	6.9	2	2	8	1	3.6	-2	8	1	3.4		
25.70	1.598	10.8	2	1	5	3	5.8	-1	5	3	4.9	24.70	1.661	8.7	2	-2	2	3	4.4	2	2	3	4.3		
27.15	1.514	17.5	1	5	3	0	7.8					25.50	1.610	11.7	2	-4	0	2	4.8	4	0	2	4.6		
27.20	1.511	23.3	2	1	9	2	7.3	-1	9	2	7.1	25.65	1.601	19.9	2	-1	5	3	8.6	1	5	3	8.4		
27.25	1.508	19.4	2	-5	1	1	4.2	5	1	1	4.1	25.70	1.598	12.5	1	4	6	0	3.4						
27.30	1.506	12.6	1	3	9	0	3.9					26.70	1.539	8.3	2	4	6	1	3.1	-4	6	1	3.1		
29.25	1.407	23.0	1	0	0	4	23.0					26.80	1.533	10.3	2	-2	8	2	4.3	2	8	2	4.2		
29.60	1.391	81.8	2	4	6	2	42.3	-4	6	2	39.2	27.05	1.519	12.2	2	-3	1	3	3.7	3	1	3	3.3		
29.90	1.377	21.8	1	0	12	0	20.5					27.20	1.511	40.4	3	5	3	0	12.4	-1	9	2	12.0	1 9 2 11.8	
34.60	1.195	3.4	1	5	9	0	3.4					27.30	1.506	22.7	2	5	1	1	5.3	-5	1	1	5.3		
36.70	1.129	4.2	1	4	12	0	4.2					27.35	1.503	15.6	1	3	9	0	5.6						
42.30	0.985	10.4	1	0	12	4	8.4					27.95	1.471	6.4	2	2	10	1	3.3	-2	10	1	3.1		
42.35	0.984	8.2	1	8	0	0	4.0					28.45	1.446	7.9	2	-1	7	3	4.0	1	7	3	3.9		
												29.20	1.410	27.5	1	0	0	4	27.5						
												29.60	1.391	100.0	2	-4	6	2	50.0	4	6	2	49.6		
												29.90	1.377	24.3	1	0	12	0	22.8						
												32.50	1.270	6.0	2	3	11	1	3.0	-3	11	1	3.0		
												34.15	1.210	7.9	2	-3	3	4	4.1	3	3	4	3.9		
												34.65	1.193	5.0	1	5	9	0	5.0						
												42.30	0.985	9.8	1	0	12	4	9.3						
												42.45	0.982	5.2	1	8	0	0	4.1						
												52.05	0.810	6.4	2	-4	6	6	3.4	4	6	6	3.0		
												52.80	0.799	3.9	1	8	12	0	2.6						
												52.90	0.798	6.0	2	4	18	2	2.7	-4	18	2	2.6		

nel, and should therefore stabilize toward lower T the high-temperature spinel-bearing assemblages that are alternative to staurolite.

Magnesiostauroelite

This early synthesized end-member has long been recognized as a high-pressure phase (Schreyer & Seifert, 1969). Fockenberg (1998) determined its stability field ($12 < P < 60$ kbar, $600 < T < 900^\circ\text{C}$) in the $\text{MgO-Al}_2\text{O}_3\text{-SiO}_2\text{-H}_2\text{O}$ system

(MASH); thermodynamic extractions from these phase-equilibrium data were made by Massonne (1995) and combined with calorimetric data by Grevel *et al.* (2002).

An interesting point in terms of phase relations is, in the Dora-Maira pyrope, the coexistence of magnesiostauroelite with the talc-clinocllore-kyanite assemblage (Fig. 1), which is a lower-temperature alternative both to magnesiostauroelite and to pyrope (+ H_2O). The complete assemblage would therefore be invariant in the Fe- and Li-free MASH system. A key-point is the existence of a stability field for the talc-staurolite pair, a rare assemblage otherwise only

Table 7. Cation site preference and site grouping in the staurolite general formula, $A_4B_4C_{16}D_4T_8O_{40}X_8$ (from Hawthorne *et al.* 1993c).

Group sites	Sites	Cations
A	M4A, M4B	Fe ²⁺ , Mg ²⁺ , □ (□ > 2)
B	T2	Fe ²⁺ , Zn ²⁺ , Co ²⁺ , Mg ²⁺ , Li ⁺ , Al ³⁺ , Fe ³⁺ (?), Mn ²⁺ , □
C	M1A, M1B, M2	Al ³⁺ , Fe ³⁺ , Cr ³⁺ , V ³⁺ , Mg ²⁺ , Ti ⁴⁺
D	M3A, M3B	Al ³⁺ , Mg ²⁺ , □ (□ > 2)
T	T1	Si ⁴⁺ , Al ³⁺
X	O1A, O1B	OH ⁻ , F ⁻ , O ²⁻

found in Antarctica (Grew & Sandiford, 1984, with $X_{Mg} = 0.4$ in staurolite). In the MASH system, the two univariant reactions bounding this field, namely clinocllore + kyanite = talc + Mg-staurolite + H₂O and talc + Mg-staurolite = pyrope + kyanite + H₂O are nearly indistinguishable within experimental uncertainty (from about 17 kbar, 780 ± 15°C, to 30 kbar, 710 ± 20°C, Chopin & Sobolev, 1995), leaving virtually no stability field for the talc–staurolite assemblage. Actually, the presence of lithium in natural systems will stabilize the staurolite-bearing assemblage with respect to others and extend the stability field of staurolite, the phase in which Li is preferentially incorporated.

The partitioning of iron and magnesium between coexisting staurolite and garnet is another remarkable feature. In classical, relatively low-pressure metamorphic terranes, staurolite is Fe-rich but the coexisting garnet has a still higher X_{Fe} . The situation is commonly but not consistently reversed in intermediate-pressure rocks, in which staurolite, although increasingly magnesian, may be more Fe-rich than the coexisting garnet. Magnesiostauroлите in the Dora-Maira high-pressure rocks is consistently more Fe-rich than the coexisting garnet (Fig. 6 in Simon *et al.*, 1997), confirming the picture obtained for staurolite proper in more Fe-rich, high-pressure rocks (Ballèvre *et al.*, 1989; Chopin *et al.*, 1991). This compositional dependence of the partitioning is well reproduced by the experimental study of Koch-Müller (1997), but not the apparent pressure dependence, which makes the Fe-Mg staurolite series a persisting thermodynamic nightmare (*cf.* Koch-Müller, 1997, with references). There are good crystal-chemical reasons to this, as shown in the following.

Crystal chemistry

Details on the complex structure and site nomenclature of staurolite can be found in Hawthorne *et al.* (1993a). In brief, the staurolite structure can be described as kyanite-like and oxide-hydroxide layers alternating along [010]. Both layers contain three independent octahedra (M) and one tetrahedron (T); they are named M1A, M1B, M2 and T1 in the kyanite-like layer and M3A, M3B, M4 and T2 in the oxide-hydroxide layer. Site preferences and grouping in the staurolite general formula are reported in Table 7 (for more detail, see Hawthorne *et al.*, 1993c).

Although truly orthorhombic samples have not yet been found in Nature, staurolite can be described as an order-dis-

order series between a completely disordered orthorhombic end-member with space group *Ccmm* and an ordered monoclinic end-member with space-group *C2/m* and β values close to 90.7° (Hawthorne *et al.*, 1993b; Oberti *et al.*, 1996). This transition is continuous, and can be modelled as second-order; the primary order parameter being $Q_{M3} [= (X_{M3A} - X_{M3B}) / (X_{M3A} + X_{M3B})]$, where X is the site occupancy], which is linearly related to the β angle. Ordering occurs also at the M4A and M4B sites, but the very low occupancies at these sites increase the scattering of the data (Hawthorne *et al.*, 1993b). The only parameters deviating from a continuous second-order transition are the x and y coordinates of the O4 oxygen, which do not converge to the special position expected in the orthorhombic space-group.

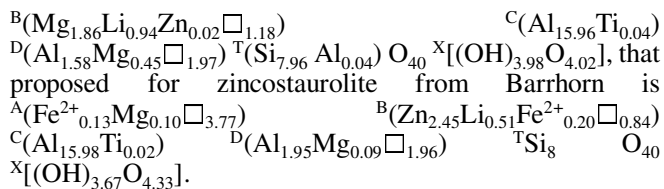
Site population

Assignment of the various chemical species to the distinct structural sites can be attempted by combining the analysis of the refined site-scattering values and site geometry with the local-ordering patterns available for the partially vacant sites (Hawthorne *et al.*, 1993c), the site preferences inferred from crystal-chemical analysis (Table 7) and the evidence obtained by spectroscopic techniques (FTIR, Mössbauer, XAS). The results of this work are slightly different from those reported in Hawthorne *et al.* (1993a) because of reconsideration of the structure refinement, of the H content and of the crystal-chemical plots. However, they are more consistent with the latest findings on cation site-preference obtained by XAS spectroscopy (Henderson *et al.*, 1993, 1997).

For the zincostauroлите sample, there is a very good agreement between the overall refined site-scattering (ss) at the cation sites (431.4 epfu) and those calculated from the unit formula reported in Table 1 (431.5 epfu). The short mean T1-O bond length (mbl, in Å), the shortest in the CNR-IGG staurolite database, suggests nearly complete Si occupancy. Refined ss and mbl at M1A, M1B and M2 suggest nearly complete Al occupancy (with the very small amount of Ti likely ordered at M2 as suggested by the XAS study of Henderson *et al.*, 1993). Zn and Li order at the T2 site, together with around 0.20 Fe apfu (as obtained from ss values); the remaining Fe and about 0.10 Mg apfu are disordered between the M4A and M4B sites, and the remaining Mg and 1.95 Al apfu are disordered between the M3A and M3B sites.

For the magnesiostauroлите sample, the agreement between refined and calculated overall site-scattering is also good (389.3 vs. 384.3 epfu, which means 1.3% deviation); it becomes excellent (385.0 vs. 384.3) when considering full Al occupancy at the M1A and M1B sites and Al + Ti occupancy at the M2 site; the latter hypothesis is confirmed by the very short mbl observed at those sites, which in our opinion precludes the presence of Mg. The same reasoning used for zincostauroлите confirms a low (not exceeding 0.05 apfu) Al content at the T1 site, with the remaining Al (1.58 apfu) and 0.45 Mg at the M3A and M3B sites; Fe²⁺ is apparently confined at the M4A and M4B sites, together with the remaining Mg (0.72 apfu).

The crystal-chemical formula proposed for magnesiostauroлите from Dora-Maira is $A(Fe^{2+}_{0.16}Mg_{0.72}\square_{3.12})$



Cation ordering

The new formula proposed for magnesiostauroilite (in which the number of vacancies, ${}^B\square$, is 1.34 times the total occupancy of the A site, ${}^A\Sigma$) confirms the suggestion that the uncoupled model for local order at the B sites, which would imply ${}^B\square = 2 \text{ } {}^M4\Sigma$, does not hold in this case (Hawthorne *et al.*, 1993a). This means that the occupied M4A and M4B sites tend to cluster; this behaviour possibly results from the high-pressure conditions of crystallization of this magnesiostauroilite. Accordingly, the same ratio calculated for the data reported by Koch-Müller *et al.* (1998) for magnesiostauroilite synthesized at 25 kbar and 700°C is 1.37.

In the magnesi- and zincostauroilite crystals of this work, the nearly equal site scattering values refined at the M1A-B, M3A-B and M4A-B pairs of sites confirm the complete disorder already suggested by the values of the β angle close to 90.0°. The degree of order in staurolites is not related to the overall composition. For instance, the zincostauroilite of this work (Zn = 2.45 pfu) is almost disordered [$\beta = 90.00(8)^\circ$ and refined site-scattering values at the M3A and M3B sites equal within su], whereas that reported by Oberti *et al.* (1996) (Zn = 2.40 pfu) is the most ordered staurolite found so far [$\beta = 90.68(2)^\circ$ and 24.67 epfu at M3A and 1.07 epfu at M3B, with Al fully ordered at M3B and Mg disordered between M3A and M3B]. The chemical composition having been excluded, a possible reason for cation ordering should be found in the crystallization conditions, especially in the kinetics of the process. However, the highly ordered staurolite described by Oberti *et al.* (1996) crystallized in metabasites of the Nevado-Filábride complex, Almeria province, Spain (sample 524-36) at proposed $T \leq 450^\circ\text{C}$ and $P < 4$ kbar (Soto & Azañón, 1994), thus under conditions very similar to those proposed for the disordered sample of this work. In addition, there is no evidence that the cooling rates in the Penninic units of the Western Alps were dramatically higher than in the Nevado-Filábride complex (it is rather the opposite: López Sánchez-Viscaíno *et al.*, 2001), and one should bear in mind that different staurolite crystals from a same sample may show quite different degrees of order [samples S(11 to 14) of Hawthorne *et al.*, 1993a]. Obviously, local rather than regional kinetic controls come in first place.

Further evidence on this topic is provided by the presence of domains that look like “cross hatched” twinning in thin sections of other prograde magnesiostauroilite inclusions in Dora-Maira pyrope megablasts (Simon *et al.*, 1998). At the TEM scale, distinct lamellar systems can be seen, parallel to either (001) or (100), some monoclinic, some pseudo-orthorhombic, and some showing superstructures along a or c (Simon *et al.*, in prep.). These features are evidence for incipient reorganization of the proton and cation distribution at a sub-crystal scale,

in spite of the extremely high exhumation (and cooling) rate of these metamorphic rocks (Gebauer *et al.*, 1997). Their unsystematic occurrence again shows the importance of the local controls (minor elements? deformation?).

Site geometry

Albeit non converging to the same value, site geometries of the pair of sites that would be equivalent in the orthorhombic space group *Ccmm*, are much more similar in the disordered zincostauroilite from Barrhorn than in the ordered zincostauroilite from Nevado Filábride ($\langle\text{M1A,B-O}\rangle = 1.909$ and 1.908 vs. 1.909 and 1.931 Å; $\langle\text{M3A,B-O}\rangle = 1.972$ and 1.977 vs. 1.952 and 2.030 Å). Of these sites, only the M1 sites are coordinated with the non-convergent O4 oxygen atoms.

The XANES studies by Henderson *et al.* (1997) showed that the local environments of 3d cations at the T2 sites are rather different, and that Fe has the most distorted and Zn a relative symmetrical site geometry. This evidence was also confirmed by EXAFS modelling, which provided refined bond lengths (R, Å) and Debye-Waller factors (DW, Å²) when using the first-shell oxygen atoms: for Fe, R = 1.99, DW = 0.023; for Co, R = 1.97–1.98, DW = 0.012; for Zn, R = 1.95–1.96, DW = 0.009; for Mg, R = 2.00, DW = 0.002. When compared with the ideal bond lengths for tetrahedral coordination based on Shannon (1976) ionic radii: 1.98 Å for Fe²⁺, 1.93 Å for Co, 1.95 Å for Zn and 1.92 Å for Mg (1.94 Å for Li), they indicate that Fe, Co and Zn occur predominantly to totally in tetrahedral coordination, whereas Mg is ordered at T2 by more than 75%. The geometry of the T2 site obtained from the structure refinement is: $\langle\text{T2-O}\rangle = 1.983$ Å, $\Delta\{[(\text{T2-O1A} + \text{T2-O1B})/2] - \text{T2-O5}\} = 0.045$ Å for zincostauroilite with ${}^T(\text{Zn}_{2.45}\text{Li}_{0.51}\text{Fe}^{2+}_{0.20}\square_{0.84})$ and $\langle\text{T2-O}\rangle = 1.981$ Å, $\Delta = 0.077$ Å for magnesiostauroilite with ${}^T(\text{Mg}_{1.86}\text{Li}_{0.94}\text{Zn}_{0.02}\square_{1.18})$. These values are absolutely consistent with the proposed site populations.

Comparison with synthetic end-members

Fockenberg (1995) studied the compositional variability of magnesiostauroilite in the MASH system with pressure increasing from 20 to 50 kbar at 800°C: H and Si contents increase from 2.5 to 3.9 and 7.7 to 8 apfu, respectively, Al contents decrease from 18.4 to 17.6 apfu, Mg passing through a maximum of 4.1 apfu at 30 kbar. The stable (?) composition in the presence of corundum at 30 kbar and 800°C is $\text{Mg}_{3.8}\text{Al}_{17.77}\text{Si}_{7.84}\text{O}_{44.86}(\text{OH})_{3.14}$, a fair agreement with the natural sample studied here if allowance is made for the presence of lithium in the latter. Koch-Müller *et al.* (1997) synthesized magnesiostauroilite and zincostauroilite at 25 kbar and 700°C and obtained best results on the molar basis $\text{Mg}_{3.8}\text{Al}_{18.3}\text{Si}_{7.6}\text{O}_{46.45}$ and $\text{Zn}_4\text{Al}_{18}\text{Si}_{7.5}\text{O}_{46}$, respectively, with water in excess. In the case of this Si-deficient magnesiostauroilite, FT-IR analysis indicated Mg incorporation at the M2 site and excluded the presence of Al at the T2 site. Later studies by Rietveld refinement (Koch-Müller *et al.*, 1998) on the same samples gave smaller Si deficiencies and 0.16 Al pfu at T2 (+ 2.12 Mg pfu); these site populations, howev-

er, are far less reliable than those obtained in this work by single-crystal refinement. Koch-Müller & Abs-Wurmbach (1996) synthesized (magnesi)stauroélites with increasing X_{Fe} from 0.15 to 1.0 working at 20 kbar, 680°C, and f_{O_2} defined by the WI buffer. Mössbauer analysis of their samples showed that Fe enters first the T2 site, and then linearly substitutes after Mg at the M4 and (M1,2) sites with nearly the same slope. Koch-Müller *et al.* (1997) also showed that increasing pressure decreases the Fe content at the T2 site and increases the Si content in T1, as for the Mg end-member. In the case of zincostauroélite, the IR spectrum was interpreted in terms of Zn incorporation at the T2 and M2 sites; low vacancy concentrations at T2 were also suggested by the absence of bands related to the H2 configuration.

The high Si contents and, therefore, near absence of tetrahedral Al in our natural samples are in keeping with the trend obtained by Fockenberg (1995) for the Mg end-member, but go far beyond those ever obtained in synthetic Zn (and Fe) end-members. One possible reason for this could be the much lower formation temperature of the natural crystal than that of the synthetic ones (*ca.* 400 vs. 700°C). The high number of protons and low Al contents of our high-pressure magnesiostauroélite are also qualitatively in excellent agreement with the trends determined by Fockenberg (1995).

Beside their nearly complete disorder which, at least for zincostauroélite, cannot be simply related to formation conditions or regional kinetic factors, another interesting feature of the natural crystals is the coordination of the divalent cation, *i.e.* the relative occupancy of the tetrahedral and octahedral sites, especially T2 vs. M4. The high-pressure magnesiostauroélite shows a lower T2 occupancy and higher M4 occupancy than any other (lower-pressure) stauroélite, as well as the highest Mg content in M3. This increasing octahedral coordination for Mg with respect to Fe and Zn is in keeping with the pressure–coordination rule. It is probably the key to the Mg-stauroélite paradox mentioned in the introduction, as well as the reason for the complex mixing behaviour of the Fe-Mg series, which has made it unamenable to a satisfying thermodynamic treatment.

Acknowledgements: We are particularly indebted to Mario Sartori, for bringing this unique metabauxite to our attention and for his enthusiastic guidance in the field, to Olaf Medenbach for optical measurements, to Detlef Lang and Rainer Altherr for the ion-microprobe analyses, to Barb Dutrow and Pierre Bariand for samples used as ion-probe standards, to Ed Grew for sharing his expertise in light elements, and to Adriana Maras and Marco Pasero for reviews.

References

- Ballèvre, M., Pinardon, J., Kiénast, J.-R., Vuichard, J.-P. (1989): Reversal of Fe-Mg partitioning between garnet and stauroélite in eclogite-facies metapelites from the Champtoceaux Nappe (Brittany, France). *J. Petrol.*, **30**, 1321-1349.
- Brugger, J., Armbruster, T., Meisser, N., Hejny, C., Grobety, B. (2001): Description and crystal structure of turtmannite, a new mineral with a 68 Å period related to megovernite. *Am. Mineral.*, **86**, 1494-1505.
- Čech, F., Povondra, P., Vrana, S. (1981): Cobaltoan stauroélite from Zambia. *Bull. Minéral.*, **104**, 526-529.
- Chopin, C. & Schertl, H.-P. (1999): The UHP unit in the Dora-Maira massif, Western Alps. *International Geology Review*, **41**, 765-780.
- Chopin, C. & Sobolev, N.V. (1995): Principal mineralogical indicators of UHP in crustal rocks. in *Ultra-high-pressure metamorphism*, R.G. Coleman & X. Wang eds., Cambridge University Press, 96-131.
- Chopin, C., Henry, C., Michard, A. (1991): Geology and petrology of the coesite-bearing terrain, Dora-Maira massif, Western Alps. *Eur. J. Mineral.*, **3**, 263-291.
- Chopin, C., Goffé, B., Ungaretti L. (1993): Magnesiostauroïde et zincstauroïde: vers la fin d'un paradoxe? [abstr.] *Bulletin de liaison, Soc. fr. Minéral. Cristallogr.*, **5**, 59.
- Chopin, C., Ferraris, G., Ivaldi, G., Schertl, H.-P., Schreyer, W., Compagnoni, R., Davidson, C., Davis, A.M. (1995): Magnesiostauortierite, a new mineral from very-high-pressure rocks (western Alps). II. Crystal chemistry and petrological significance. *Eur. J. Mineral.*, **7**, 525-535.
- Compagnoni, R., Hirajima, T., Chopin, C. (1995): Ultrahigh-pressure metamorphism in the western Alps. in *Ultra-high-pressure metamorphism*, R.G. Coleman & X. Wang eds., Cambridge University Press, 206-243.
- Dutrow, B., Holdaway, M.J., Hinton, R.W. (1986): Lithium in stauroélite and its petrological significance. *Contrib. Mineral. Petrol.*, **94**, 496-506.
- Enami, M. & Zang, Q. (1988): Magnesian stauroélite in garnet-cordierite rocks and eclogite from Donghai district, Jiangsu province, east China. *Am. Mineral.*, **73**, 48-56.
- Feenstra, A., Ockenga, E., Rhede, D. (2002): Li-H-rich zincostauroélite in a polymetamorphic high-P, low-T diaspore-bearing metabauxite from E-Samos, Greece: an EMP and SIMS study. I.M.A. 18th general meeting, Abstr. vol., 208-209.
- Fockenberg, T. (1995): Synthesis and chemical variability of Mg-stauroélite in the system MgO-Al₂O₃-SiO₂-H₂O as a function of water pressure. *Eur. J. Mineral.*, **7**, 1373-1381.
- (1998): An experimental investigation on the P-T stability of Mg-stauroélite in the system MgO-Al₂O₃-SiO₂-H₂O. *Contrib. Mineral. Petrol.*, **130**, 187-198.
- Gebauer, D., Schertl, H.-P., Brix, M., Schreyer, W. (1997): 35 Ma old ultrahigh-pressure metamorphism and evidence for rapid exhumation in the Dora Maira massif, Western Alps. *Lithos*, **41**, 5-24.
- Gil Ibarguchi, J.I., Mendia, M., Girardeau, J. (1991): Mg- and Cr-rich stauroélite and Cr-rich kyanite in high pressure ultrabasic rocks (Cabo Ortegal, northwestern Spain). *Am. Mineral.*, **76**, 501-511.
- Goffé, B. (1980): Magnésiocarpholite, cookéite et euclase dans les niveaux continentaux métamorphiques de la zone Briançonnaise. Données minéralogiques et nouvelles occurrences. *Bull. Minéral.*, **103**, 297-302.
- (1984): Le faciès à carpholite-chloritoïde dans la couverture Briançonnaise des Alpes Ligures: un témoin de l'histoire tectono-métamorphique régionale. *Mem. Soc. geol. It.*, **28**, 461-479.
- Goffé, B. & Saliot, P. (1977): Les associations minéralogiques des roches hyperalumineuses du Dogger de Vanoise. Leur signification dans le métamorphisme régional. *Bull. Soc. fr. Minéral. Cristallogr.*, **100**, 302-309.
- Goffé, B. & Velde, B. (1984): Contrasted metamorphic evolutions in the thrust cover units of Briançonnais zone (French Alps): a model for the conservation of HP-LT metamorphic mineral assemblages. *Earth Plan. Sci. Lett.*, **68**, 351-360.
- Grevel, K.-D., Navrotsky, A., Fockenberg, T., Majzlan, J. (2002): The enthalpy of formation and internally consistent thermodynamic data of Mg-stauroélite. *Am. Mineral.*, **87**, 397-404.

- Grew, E.S. (2002): Beryllium in metamorphic environments (with an emphasis on aluminous compositions). in Beryllium, E.S. Grew ed. *Reviews in Mineralogy and Geochemistry*, **50**, in press.
- Grew, E.S. & Sandiford, M. (1984): A staurolite-talc assemblage in tourmaline-phlogopite-chlorite schist from northern Victoria Land, Antarctica, and its petrogenetic significance. *Contrib. Mineral. Petrol.*, **87**, 337-350.
- Grew, E.S., Hinthorne, J.R., Marquez, N. (1986): Li, Be, B, and Sr in margarite and paragonite from Antarctica. *Am. Mineral.*, **71**, 1129-1134.
- Griffen, D.T. (1981): Synthetic Fe/Zn staurolites and the ionic radius of $^{IV}Zn^{2+}$. *Am. Mineral.*, **66**, 932-937.
- Hawthorne, F.C., Ungaretti, L., Oberti, R., Caucia, F., Callegari, A. (1993a): The crystal-chemistry of staurolites. I: Crystal structure and site populations. *Can. Mineral.*, **31**, 551-582.
- , –, –, – (1993b): The crystal-chemistry of staurolites. II: Order-disorder and the monoclinic orthorhombic phase transition. *Can. Mineral.*, **31**, 583-596.
- , –, –, – (1993c): The crystal-chemistry of staurolites. III: Local order and chemical composition. *Can. Mineral.*, **31**, 597-616.
- Henderson, C.M.B., Charnock, J.M., Smith, J.V., Greaves, G.N. (1993): X-ray absorption spectroscopy of Fe, Mn, Zn and Ti structural environment in staurolite. *Am. Mineral.*, **78**, 477-485.
- Henderson, C.M.B., Charnock, J.M., Cressey, G., Griffen, D.T. (1997): An EXAFS study of the local structural environments of Fe, Co, Zn and Mg in natural and synthetic staurolites. *Mineral. Mag.*, **61**, 613-625.
- Holdaway, M.J., Dutrow, B.L., Shore, P. (1986): A model for the crystal chemistry of staurolite. *Am. Mineral.*, **71**, 1142-1159.
- Koch-Müller, M. (1997): Experimentally determined Fe-Mg exchange between synthetic staurolite and garnet in the system $MgO-FeO-Al_2O_3-SiO_2-H_2O$. *Lithos*, **41**, 185-212.
- Koch-Müller, M. & Abs-Wurmbach, I. (1996): Crystal-chemistry of synthetic Fe-Mg staurolite, investigated by Mössbauer-spectroscopy. *Phys. Chem. Minerals*, **23**, 239-240.
- Koch-Müller, M., Langer, K., Behrens, H., Schuck, G. (1997): Crystal chemistry and infrared spectroscopy in the OH-stretching region of synthetic staurolites. *Eur. J. Mineral.*, **9**, 67-82.
- Koch-Müller, M., Kahlenberg, V., Bubenik, W., Gottschalk, M. (1998): Crystal-structure refinement of synthetic Fe- and Mg-staurolite by Rietveld analysis of X-ray powder diffraction data. *Eur. J. Mineral.*, **10**, 453-460.
- Leupolt, L. & Franz, G. (1986): Zink-Staurolith aus Metasedimenten der Eklogitzone, Tauern/Österreich. *Fortschr. Mineral.*, **64**, Bh. 1, 96.
- Lonker, S.W. (1983): The hydroxyl content of staurolite. *Contrib. Mineral. Petrol.*, **84**, 36-42.
- López Sánchez-Viscaíno, V., Rubatto, D., Gómez-Pugnaire, M.T., Trommsdorff, V., Müntener, O. (2001): Middle Miocene high-pressure metamorphism and fast exhumation of the Nevado-Filábride complex, SE Spain. *Terra Nova*, **13**, 327-332.
- Massonne, H.-J. (1995): Experimental and petrogenetic study of UHPM. in Ultra-high-pressure metamorphism, R.G. Coleman & X. Wang eds., Cambridge University Press, 33-95.
- Nicollet, C. (1986): Sapphirine et staurolite riche en magnésium et chrome dans les amphibolites et anorthosites à corindon du Vohibory sud, Madagascar. *Bull. Minéral.*, **109**, 599-612.
- Oberti, R., Hawthorne, F.C., Zanetti, A., Ottolini, L., Soto, J.I. (1996): Crystal-structure refinement of a highly ordered staurolite. *Can. Mineral.*, **34**, 1051-1057.
- Peacock, S.M. & Goodge, J.W. (1995): Eclogite-facies metamorphism preserved in tectonic blocks from a lower crustal shear zone, Transantarctic Mountains, Antarctica. *Lithos*, **36**, 1-13.
- Poinssot, C., Goffé, B., Toulhoat, P. (1997): Geochemistry of the Triassic-Jurassic Alpine continental deposits: origin and geodynamic implications. *Bull. Soc. géol. Fr.*, **168**, 287-300.
- Sartori, M. (1988): L'unité du Barrhorn (zone pennique, Valais, Suisse). Un lien entre les Préalpes médianes rigides et leur socle paléozoïque. Thèse de doctorat, Université de Lausanne, 157 p.
- Schreyer, W. & Seifert, F. (1969): High-pressure phases in the system $MgO-Al_2O_3-SiO_2-H_2O$. *Am. J. Sci.*, **267-A**, 407-443.
- Schreyer, W., Horrocks, P.C., Abraham, K. (1984): High-magnesium staurolite in a sapphirine-garnet rock from the Limpopo Belt, Southern Africa. *Contrib. Mineral. Petrol.*, **86**, 200-207.
- Shannon, R.D. (1976): Revised effective ionic radii and systematic studies of interatomic distances in halides and chalcogenides. *Acta Crystallogr.*, **A32**, 751-767.
- Simon, G. & Chopin, C. (2001): Enstatite-sapphirine crack-related assemblages in ultrahigh-pressure pyrope megablasts, Dora-Maira massif, western Alps. *Contrib. Mineral. Petrol.*, **140**, 422-440.
- Simon, G., Chopin, C., Schenk, V. (1997): Near-end-member magnesiochloritoid in prograde-zoned pyrope, Dora-Maira massif, western Alps. *Lithos*, **41**, 37-57.
- Simon, G., Chopin, C., Czank, M., (1998): Magnesio-staurolite in UHP rocks: a HP phase with some uncommon features. 17th IMA general meeting, Toronto, Abstract vol., 100.
- Skerl, A.C. & Bannister, F.A. (1934): Lusakite, a cobalt-bearing silicate from Northern Rhodesia. *Mineral. Mag.*, **23**, 598-606.
- Smith, D.C. (1988): A review of the peculiar mineralogy of the "Norwegian-eclogite province", with crystal-chemical, petrological, geochemical and geodynamical notes and an extensive bibliography. in Eclogites and eclogite-facies rocks. Elsevier, Amsterdam, 1-206.
- Soto, J.I. & Azañón, J.M. (1993): The breakdown of Zn-rich staurolite in a metabasite from the Betic Cordillera (SE Spain). *Mineral. Mag.*, **57**, 530-533.
- & – (1994): Zincian staurolite in metabasites and metapelites from the Betic Cordillera (SE Spain). *Neues Jahrb. Mineral. Abh.*, **168**, 109-126.
- Stoddard, E.F. (1979): Zinc-rich hercynite in high-grade metamorphic rocks: a product of the dehydration of staurolite. *Am. Mineral.*, **64**, 736-741.
- Vidal, O. & Goffé, B. (1991): Cookeite, $LiAl_4(Si_3Al)O_{10}(OH)_8$: experimental study and thermodynamic analysis of its compatibility relations in the $Li_2O-Al_2O_3-SiO_2-H_2O$ system. *Contrib. Mineral. Petrol.*, **108**, 72-81.
- Ward, C.M. (1984): Magnesium staurolite and green chromian staurolite from Fjordland, New Zealand. *Am. Mineral.*, **69**, 531-540.

Received 24 February 2002

Modified version received 17 September 2002

Accepted 22 October 2002